

Monthly and Daily Variations in down ward Long wave Radiation and Its Relationship with Atmospheric Temperature and Water Content in desert and Mediterranean Climates

Maghrabi A.H.^{*1} and Odah S. H².

¹National Centre for Applied Physics, King Abdulaziz City for Science and Technology, Riyadh 11442, Saudi Arabia.

²Physics and Astronomy Department, King Saud University, Riyadh, Saudi Arabia
Corresponding Author: Maghrabi A.H.

Abstract: Knowledge of downward atmospheric radiation in the range $\lambda = 4-100 \mu\text{m}$ is vital for several applications. In this study, longwave (LW) radiation data from desert (Riyadh, Saudi Arabia) and Mediterranean (Adelaide, Australia) climates are used to characterize seasonal and daily variations.

At both sites, the LW radiation shows a maximum in summer and a minimum in winter. The monthly changes in the LW radiation were about 22% for Adelaide, and 36% for Riyadh. When considering these seasonal variations, it was found that during winter and summer, the variations in LW radiation were confined to between 2% and 4%. However, during the transition seasons (spring and autumn) the LW radiation varies considerably. In Adelaide, spring and autumn change by about 8% and 10% respectively. In Riyadh, the LW radiation varies by about 12% in both seasons.

At both sites, the LW radiation has a minimum value in the early morning, around 06:00 local time, and reaches its maximum at around 13:00. The daily changes in the LW radiation were 13.5% for Riyadh and 10% for Adelaide.

Obviously, the monthly and diurnal variations of the LW radiation closely follow the temperature variations rather than the water content.

The influence of screen temperature (T) and atmospheric moisture on LW radiation are examined for each site. The screen level water vapour pressure (e) and the precipitable water vapour (PWV) are used as two different representative measures of the atmospheric water contents. PWV is calculated using radiosonde observations from both sites. It is clear that the LW radiation correlates better with T than e , and better correlation between LW and e was apparent in Adelaide than in Riyadh. When using the PWV as a measure of the total atmospheric water content, the correlation between LW radiation and this variable improves significantly for both sites.

Regression analyses are carried out between LW radiation and temperature and water vapour pressure at screen level (T , e), LW radiation and screen temperature and PWV (T , PWV) for each site individually, and data are combined from both sites. Statistical indicators such as mean bias error (MBE), root mean square error (RMSE), mean percentage error (MPE), and student t -tests are used to assess these regressions. Both schemes give good predictions for the measured data, although the model containing (T , PWV) shows better statistics (better predictions) for the three datasets in comparisons with the model using (T , e). For instance, the model containing (T , e) gives a RMSE of 19.38 Wm^{-2} for Riyadh, 20.52 Wm^{-2} for Adelaide, and 22.419 Wm^{-2} for the combined data from both sites. Using the scheme comprising (T , PWV) reduces the RMSE values by 16% for Adelaide, 34% for Riyadh, and 14% for the combined data.

Finally, several previously developed models are used to calculate the LW radiation for the three datasets (Adelaide, Riyadh, and the combined data from both sites). Nineteen models with different functional forms and different meteorological variables are selected and used. We find that the predictability of these models varies from one dataset to another. While some models show adequate prediction for one site, they fail for the other. However, some models give reasonable estimates when the measured data from both sites are combined.

Keywords: Meteorology; Longwave Radiation; Climate; PWV; Screen temperature; monthly variations; daily variations.

Date of Submission: 12-01-2019

Date of acceptance: 27-01-2019

I. Introduction

Downward longwave (LW) radiation is due to absorption and emission caused by greenhouse gases (GHG) in the infrared wavelengths ($\lambda = 4-100 \mu\text{m}$). Among these gases are water vapour, carbon dioxide and certain trace gases such as ozone and methane. The amount of emitted radiation depends on the distribution of

these gases (Angstrom 1915; Idso and Jackson 1969; Berdahl and Fromberg 1982; Heitor et al., 1991). The determination of LW radiation is of great importance in several applications such as atmospheric science, meteorology, radiation budget studies, and climatological studies (Stephens 1984; Wild et al., 2001). LW radiation data can be obtained using measuring equipment such as pyrgeometers. However, due to the cost of maintenance and the necessary calibration procedures of this type of equipment, LW data are always not obtainable (e.g., Berdahl and Fromberg 1982; Miskolczi 1993; Philipona et al., 2001; Duarte 2006).

Empirical correlations between LW radiation and easy-to-measure meteorological variables are usually conducted when these data are scarce. Several models have been developed using this approach. Temperature and water vapour are the most commonly used variables in these models, and different functional forms have been suggested to calculate the LW radiation under different climatic conditions (Berdahl and Martin 1984; Dilley and O'Brien 1998; Crawford and Duchon 1999; Jin et al., 2006; Ruckstuhl et al., 2007; Bilbao and De Miguel 2007; Dupont et al., 2008; ViAdex-Mora et al., 2009).

In this study, LW radiation data from a Mediterranean climate (Adelaide, Australia) and a desert climate (Riyadh, Saudi Arabia) are used to study and characterize the seasonal and diurnal variations in the LW radiation. Additionally, the effects of temperature at screen level and atmospheric water contents (at screen level and integrated over the whole atmospheric profile) under clear skies are established for both sites. Several previously proposed models will be assessed in terms of their predictability for the three datasets.

II. Experimental Data and Methodology

2.1 Description of Sites

Adelaide (34.9 S, 130.6 E, 4 m) is located in the southern part of the Australian continent and can be described as having a Mediterranean climate. Adelaide is characterized by warm-to-hot, dry summers (December to February), and mild-to-cool winters (June to August) with moderate rainfall. The mean daytime temperature is about 31°C, although there are several occasions when it experiences maximum temperatures of 42°C or above. During winter, the temperature ranges between 6–15°C with frequent frosts, mainly in the valleys of the Adelaide Hills.

Riyadh (24.35 N, 46.42 E, 620 m) is the capital, largest and most populated city in Saudi Arabia. It is located in the centre of the Arabian Peninsula, and has a hot, arid, desert climate. In summer, very low humidity is usually recorded in Riyadh, and the mean daytime temperature is between 43–46 °C, with some days when the temperature exceeds 51°C. During winter, the climate is warm, with cool, windy nights. The mean temperature at night is between 10–14°C, and zero temperatures are rarely seen in Riyadh. The large temperature variations between these seasons in Riyadh are due to the arid conditions and the prevalence of continentality. Riyadh is also characterized by a high frequency of dust storm events and occurrences of moderate rain fall, particularly during the pre-monsoon season.

2.2 Observational Data

The data used in this study comprises LW radiation measurements, surface meteorological and radiosonde observations.

For the Adelaide site, LW radiation at 4–50 μm was measured for the period between 2003 and 2006, using the CGR1 pyrgeometer developed by Kipp and Zonen (2000). The detector was installed at Kent Town weather station (centre of Adelaide City, approximately 10 km from the coast) and measured the hemispherical LW radiation with a sampling frequency of 1 Hz, collected as 30 minute averages.

Standard meteorological observations of ground temperature, dew point temperature, air pressure and cloud data were obtained from Adelaide Airport (8 km from the city centre) and records were made by the Australian Bureau of Meteorology.

LW radiation and meteorological measurements for Riyadh city, for the period between 2014 and 2016, were obtained from the King Abdulaziz City for Science and Technology (KACST) station installed on the rooftop of the Applied Physics Centre building at KACST. The LW radiation was measured using the CGR4 pyrgeometer from Kipp and Zonen (2013). The measurements were acquired with a sampling frequency of 10 Hz and stored as 10 min averages. Meteorological parameters were measured using the Skye Mini Met station (Skye Instruments, 2013). For consistency, hourly averaged data from both sites were considered.

Clear sky times were selected based on the cloud information provided by the Australian Bureau of Meteorology (ABM) and the Saudi Presidency of the Environment (SPE). The cloud coverage was required to be less than two octas during the course of measurements.

Table 1 presents the mean, maximum, minimum and standard deviation values of the LW measurements and some meteorological data for both Adelaide and Riyadh.

The mean temperature (T) in Riyadh is 10°C warmer than for Adelaide. In addition, the mean LW radiation in Riyadh is about 69 W/m² higher than that measured in Adelaide. In contrast, the mean relative

humidity (RH) in Adelaide is four times higher than in Riyadh. The mean total atmospheric water content in Riyadh is slightly higher than that found in Adelaide.

Table 1. Basic statistical parameters for screen level temperature, pressure, relative humidity, precipitable water vapour and LW radiation during clear sky periods for Adelaide (22610 hours for screen level parameters and 945 hours for PWV data) and Riyadh (1141 hours for screen level parameters and 780 hours for PWV data) during the periods considered

		<i>T</i> [°C]	<i>e</i> [mbar]	<i>RH</i> [%]	<i>P</i> [mbar]	<i>PWV</i> [mm]	<i>LW</i> [Wm ⁻²]		<i>T</i> [°C]	<i>e</i> [mbar]	<i>RH</i> [%]	<i>P</i> [mbar]	<i>PWV</i> [mm]	<i>LW</i> [Wm ⁻²]
Mean	Adelaide	18.51	10.35	52.31	1017.59	16.20	325.47	Riyadh	29.5	8.33	12.00	939.23	18.57	393.63
Standard Deviation		7.39	3.51	22.19	7.04	7.80	37.34		9.25	3.52	19.26	3.90	6.55	47.25
Minimum		-0.10	0.49	2.00	993.80	4.24	248		3.41	1.71	3.37	929.53	2.64	247.47
Maximum		43.00	26.60	100.00	1039.	59.95	472		45.98	21.97	99.99	951.09	41.59	589.80

2.3 Methodology

We first consider the diurnal and monthly behaviours of the LW radiation and the meteorological variables, primarily the temperature and the water contents. The mean values of these variables were classified into 12 bins to study their monthly variations and into 24 bins to investigate the daily variation.

The relationship between the measured LW atmospheric radiation, temperature and the water content was then investigated for each site separately and by combining the data from both sites. Statistical estimators such as the mean percentage error (MPE), mean bias error (MBE), root mean square error (RMSE), student t-test and correlation coefficient (R) were used to assess the association between these variables.

The effect of the atmospheric water content on LW radiation was investigated using the screen level vapour pressure and the total integrated water content, namely the PWV. Radiosonde measurements provided by ABM and SPE for the considered periods were used to calculate the PWV values for each site as follows (e.g., Maghrabi and Clay 2010):

$$PWV = \int_0^z \rho_v(z) dz \tag{1}$$

where ρ_v is the absolute humidity at level z . For each radiosonde profile, the required data were extracted at every available atmospheric level, and Equation (1) was integrated to calculate the PWV for the whole atmospheric profile. The calculated statistical parameters for this variable for each site are given in Table 1.

III. Results and Discussion

3.1 Monthly Variation

Figures 1 to 4 present the monthly and diurnal variations in LW radiation, air temperature, vapour pressure and PWV for the two sites. The monthly and diurnal variations in the LW radiation and air temperature are typical for the climates of Adelaide (southern hemisphere) and Riyadh (northern hemisphere) and are comparable to the observed pattern in other places with the same climate (e.g., Alados-Arboledas, and Jimenez, 1988 and Sicart et al, 2010 for northern hemisphere; and Barbaro et al 2010, for southern hemisphere).

Monthly variations are generally characterized by high LW radiation and temperatures in summer and low values in winter. The variations in the LW radiation, air temperature, vapour pressure, and PWV in Adelaide were 22%, 158%, 59% and 45% respectively. LW radiation shows a maximum in January ($356 \pm W/m^2$); between February and March, it drops by about $17 W/m^2$ (6%), and then decreases gradually until it reaches a minimum (about $290 W/m^2$) in winter. The monthly patterns for the three meteorological variables are similar to that of the LW radiation. It should be noted that the temperature between May and June fell by 46%, while the PWV dropped by about 38% between February and March. The LW radiation pattern reflects the effect of the local climate on both temperature and moisture. While the variations in LW radiation during winter and summer were 2% and 3% respectively, the variations in spring (7.8%) and autumn (9.7%) were larger.

The monthly variations in LW radiation, temperature, vapour pressure and PWV for Riyadh were 36%, 24%, 146% and 78%, respectively. The LW radiation pattern in Riyadh is somewhat similar to that of Adelaide, as it follows the trend of air temperature. However, it varies considerably throughout these seasons. For instance, in spring (March to May) and autumn (September to November), the LW radiation changes by about 12%, whereas it ranges between 3%–4% during the winter and summer seasons. Additionally, large changes in the LW radiation are evident between the last and the first months of a transition season. For instance, the change in LW radiation between February and March (transition from winter to summer) and between November and December (transition from autumn to winter) was about 15%. These larger variations during the transition seasons reflect the effect of the instability in the atmospheric conditions during these times. For instance, spring in Riyadh begins with continuous episodes of dust storms.

The seasonal pattern in the vapour pressure and PWV in Riyadh is different from that in Adelaide, as it somewhat fails to follow the pattern of the temperature. The vapour pressure decreases slowly from December until it reaches a minimum of 5.2 mbar in July. It then increases to a maximum in November, and decreases by about 68% to reach a value of about 7.8 mbar in December.

The monthly variation in the PWV shows two minima and two maxima. The first minimum in PWV occurs in February (12.5 mm), and it then jumps by about 73% to reach the first maximum in March (22 mm). It then decreases to the second minimum (15.4 mm) in July. An increasing trend is then shown in the PWV, to reach the second maximum (25.7 mm) in October. It is noticeable that the PWV increases by about 31% between September and October.

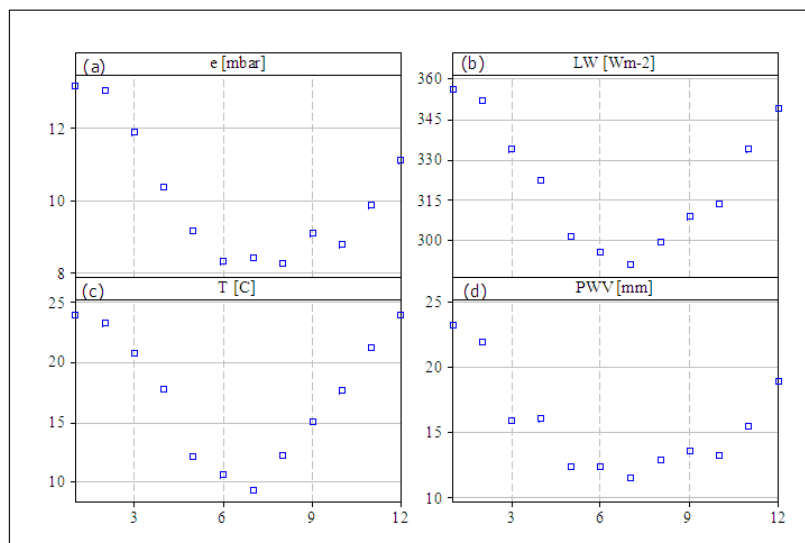


Fig.1. Monthly cycles in: (a) screen level vapour pressure; (b) LW radiation; (c) screen level temperature; and (d) PWV for the Adelaide site

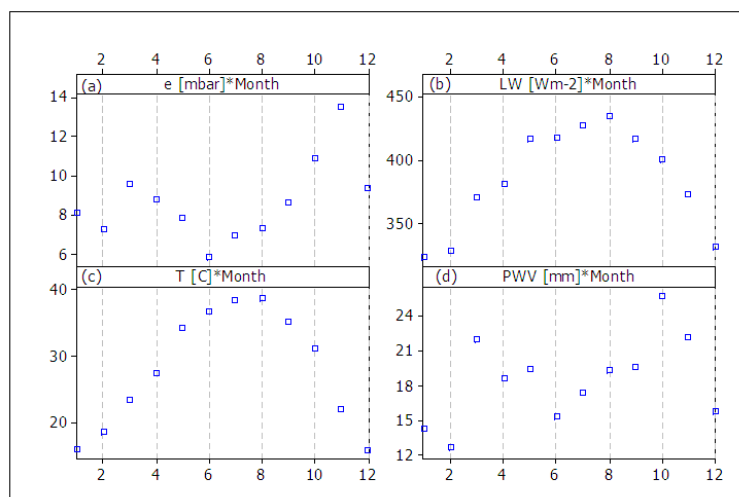


Fig.2. As Fig. 1, but for the Riyadh site.

3.2 Diurnal Variations

Figures 3 and 4 indicate the daily variations in LW radiation, vapour pressure and air temperature for both sites. It is clear that the daily variation in the LW radiation follows that of the temperature. Both variables have minimum values in the early morning (06:00 local time), and these then gradually increase to reach a maximum at around 13:00. The two variables then start to decrease gradually after 13:00 in Riyadh, although they plateau around their maximum values for between two and three hours in Adelaide. The daily variations in temperature and LW were 34% and 13.5% respectively for Riyadh, and 87% and 10% for Adelaide.

In Riyadh, water vapour pressure varies by about 18%, and in Adelaide by 14%. In Riyadh, it shows a gradual increasing trend from 15:00 local time, reaching its maximum at around 05:00. It then decreases slightly to a minimum of 7.5 mbar at 14:00. In Adelaide, the variation in the water vapour pressure is entirely different from Riyadh. It increases from 9.5 mbar at 05:00 to reach a maximum of 11 mbar at 20:00, and it then decreases again.

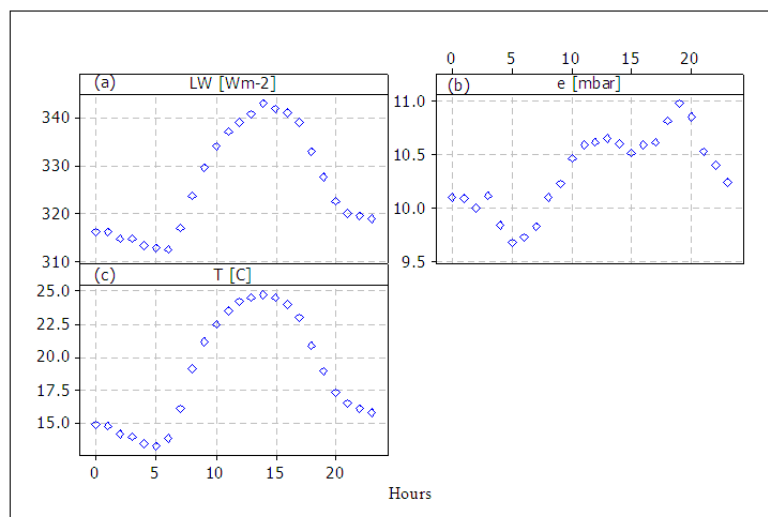


Fig.3. Hourly variation in: (a) LW radiation; (b) screen level vapour pressure; and (c) screen level temperature, for the Adelaide site.

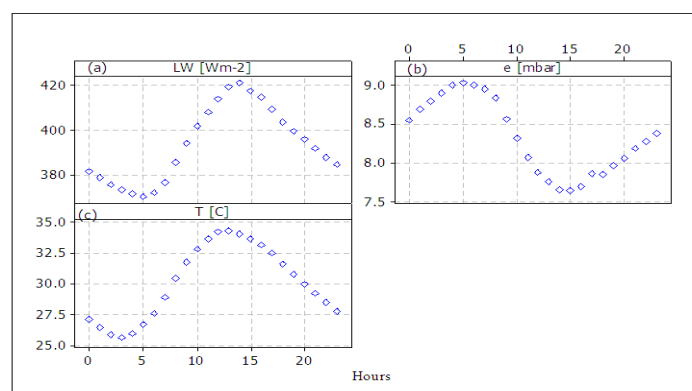


Fig. 4. As Fig 3, but for the Riyadh site.

3.3 Relationship between LW Radiation, Screen Level Temperature and Water

Figures 5 and 6 show the hourly data for the LW radiation, plotted against the screen temperature and water vapour pressure for Riyadh and Adelaide, respectively. It is clear that the LW radiation at both sites has a better correlation with screen temperature than with water vapour pressure. The correlation coefficient and the RMSE between the LW radiation and the screen temperature were 0.88 and 22 Wm^{-2} respectively for Riyadh, and 0.81 and 22 Wm^{-2} for Adelaide. However, LW radiation shows a better correlation with the vapour pressure in Adelaide than that found in Riyadh. For Adelaide, the correlation coefficient was 0.4, and the RMSE was 35 Wm^{-2} , whereas the correlation coefficient and RMSE for Riyadh were 0.2 and 48 Wm^{-2} respectively.

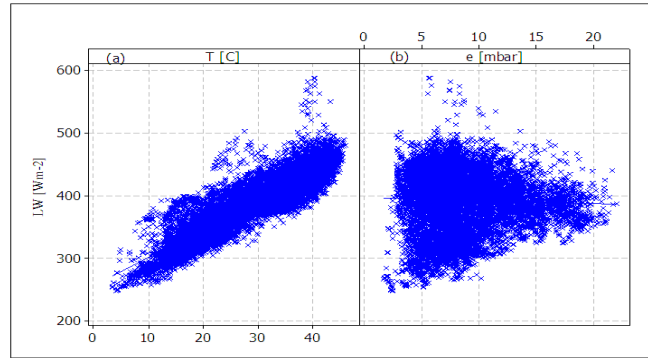


Fig.5.Scatter plot for(a) LW radiation and screen temperature; and (b) LW and screen level vapour pressure for the Riyadh site

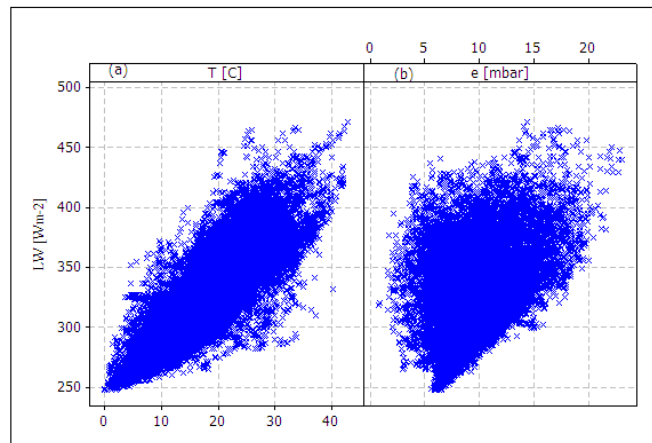


Fig. 6.As Fig. 5, but for the Adelaide site.

Regression analyses were carried out for LW radiation data and both variables for Riyadh, Adelaide, and the combined data from both sites; these gave the following equations:

$$LW(T, e) = 222.9171 + 4.8409 \times T + 2.9826 \times e \text{ (Riyadh) (2)}$$

$$LW(T, e) = 229.804 + 3.8252 \times T + 2.4045 \times e \text{ (Adelaide) (3)}$$

$$LW(T, e) = 222.6917 + 4.8592 \times T + 1.734 \times e \text{ (Both sites) (4)}$$

The regression results and the statistical indicators for these equations are given in Table 2. In all cases, the slopes of the regression between the measured and the predicted values are close to one; MBE is very small; the MPE is less than 0.5%; and t-values are less than the critical values (less than one) at a 95% level of significance for (n-1) degrees of freedom. The RMSE was 19.38 Wm⁻² for Riyadh (5% of the mean), 20.52 Wm⁻² for Adelaide (5% of the mean), and 22.419 Wm⁻² (6% of the mean) for the combined data.

Table 2. Statistical results for the regression analyses (Eqs. 2 to 4) between the hourly LW radiation and the screen level temperature and water vapour pressure for the three datasets

	Riyadh	Adelaide	Combined Data
MBE	-0.0003	0.0003	-0.0001
MPE	-0.24	-0.36	-0.38
RMSE	19.38	20.52	22.38
R	0.85	0.78	0.86
Slope	0.89	0.76	0.84
t-values	0.002	0.002	0.001
n-1	11392	22568	33961

The relationship between the measured and calculated LW radiation in the three models is depicted in Figure 7. It is clear that all the models predict the measured data with good accuracy. For most cases, about 95% of the predicted LW radiation data are in close agreement with the measured data. The failure of the models to predict the measured data in some situations may be due to the uncertainties associated with measurements of the meteorological variables and/or LW radiation. Other atmospheric parameters not considered here, such as the effects of atmospheric aerosols, wind speed and high level clouds, may have major influences on the LW radiation in some situations (Riodran et al., 2005; Sugita and Brutsaert 1993). Moreover, the day/night variations in the atmospheric boundary layer may affect the contribution of the screen level water contents to the absorption and re-emission of LW radiation (Kruk et al., 2010). This explanation will be justified in the following section when the total atmospheric water content, PWV, is used instead of the screen level water.

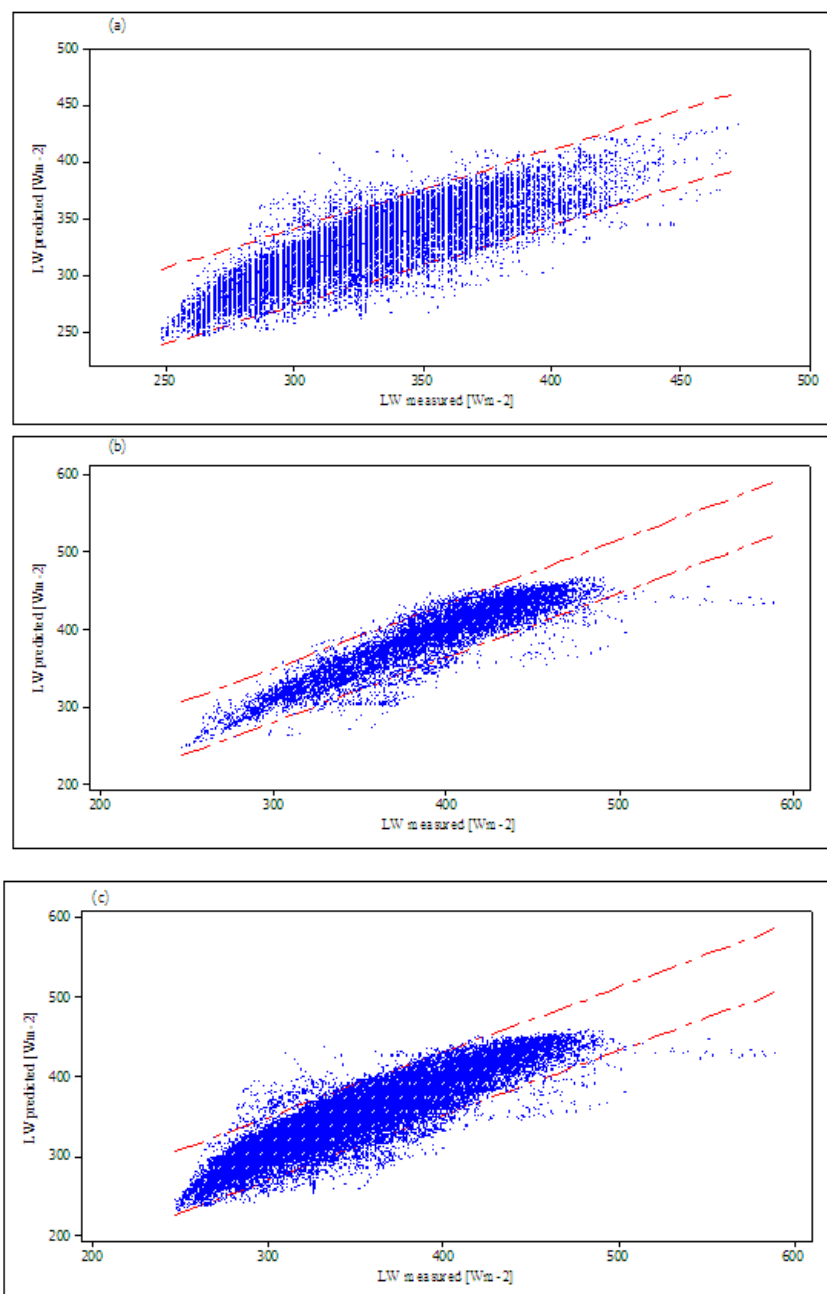


Fig.7. Scatter plot of the measured and predicted LW radiation for: (a) Adelaide data; (b) Riyadh data; and (c) combined data from both sites. The dashed red lines represent the 95% confidence interval

3.4 Relationship between LW Radiation, Screen Level Temperature and Total Water Content

Precipitable water vapour (PWV) is generally used as an actual measure of the total moisture in the atmosphere. Several researchers have suggested that PWV is a more suitable variable for investigating the real influence of the atmospheric water on LW radiation (Dilley and O'Brien 1998; Prata 1996; Dupont et al., 2008). In this section, the dependence of the LW radiation on PWV will be investigated, and an alternative scheme for modelling the LW radiation using the screen temperature and the PWV will be developed.

Radiosonde data from both sites over the considered time periods were used to calculate the PWV using Equation (1). A total of 945 PWV data points from the Riyadh site and 780 from the Adelaide site were available for the purpose of this work. The basic statistics of the calculated PWV data are given in Table 1. The corresponding meteorological variables and LW radiation data for the times that have PWV data were selected.

The mean values and statistical values for the selected data did not differ significantly from the values presented in Table 1.

Figure 8 presents the relationship between the LW radiation and the radiosonde-derived PWV for both the Riyadh and Adelaide sites. It can be seen that the relationship between the LW radiation and the atmospheric water contents, as represented by PWV, is significantly improved when compared with using the screen level water vapour (Figures 5 and 6). The correlation coefficient and RMSE were 0.71 and 26.02 Wm⁻² respectively for Adelaide and 0.48 and 38 Wm⁻² for Riyadh.

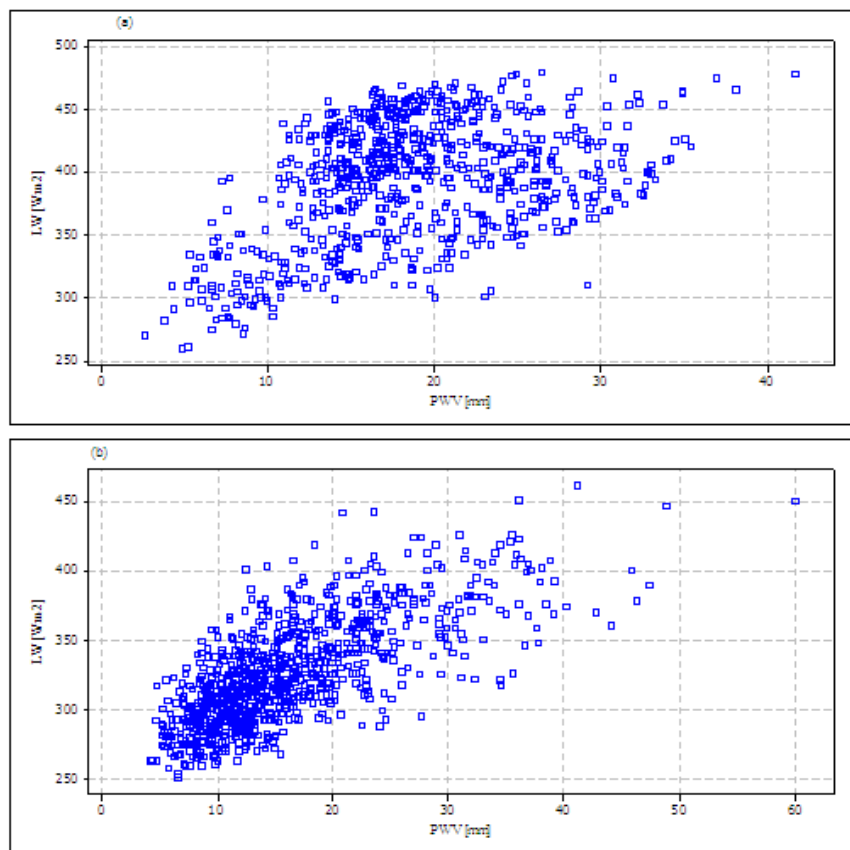


Fig. 8 Scatter plot of LW radiation and precipitable water vapour (PWV) data for (a) Adelaide and (b) Riyadh .

Multiple regression analyses between the LW radiation and both the screen temperature and PWV for the three groups of data give the following equations:

$$LW (T, PWV) = 222.51 + 4.51 T + 1.93 PWV \quad (\text{Riyadh}) \quad (5)$$

$$LW (T, PWV) = 239.68 + 2.99 T + 1.86 PWV \quad (\text{Adelaide}) \quad (6)$$

$$LW (T, PWV) = 222.43 + 4.48 T + 1.57 P \quad (\text{Both Sites}) \quad (7)$$

The statistical results of these equations are presented in Table 3. It is noticeable that the use of PWV, as a representative of atmospheric water, improves the prediction of the LW radiation significantly. For

instance, the RMSE values have been reduced by 16% for Adelaide, 34% for Riyadh, and 14% for the combined data when the PWV is used rather than the screen level vapour pressure. The slopes of the regressions between the measured and the predicted data are 0.9 for Riyadh, 0.82 for Adelaide and 0.89 for the combined data. The MPE for all three datasets was less than 1%, and the t-values were less than the critical values at a 95% level of significance.

Table 3. Statistical results for regression analyses (Eqs. 5–7) between the hourly LW radiation and the screen level temperature and PWV for the three datasets

	Riyadh	Adelaide	Combined
MBE	0.0006	0.0003	0.0005
MPE	-0.14	-0.28	-0.27
RMSE	14.79	17.10	19.54
R	0.87	0.95	0.93
Slope	0.90	0.82	0.89
t-stat	0.0011	0.0005	0.0011
n-1	755	940	1696

Figure 9 shows the relationship between the measured and the calculated LW radiation from the three parameterizations (Eqs. 5–7). It is clear that all the models predict the measured data with good accuracy. The data fall entirely or close to the 95 % confidence line for all three models.

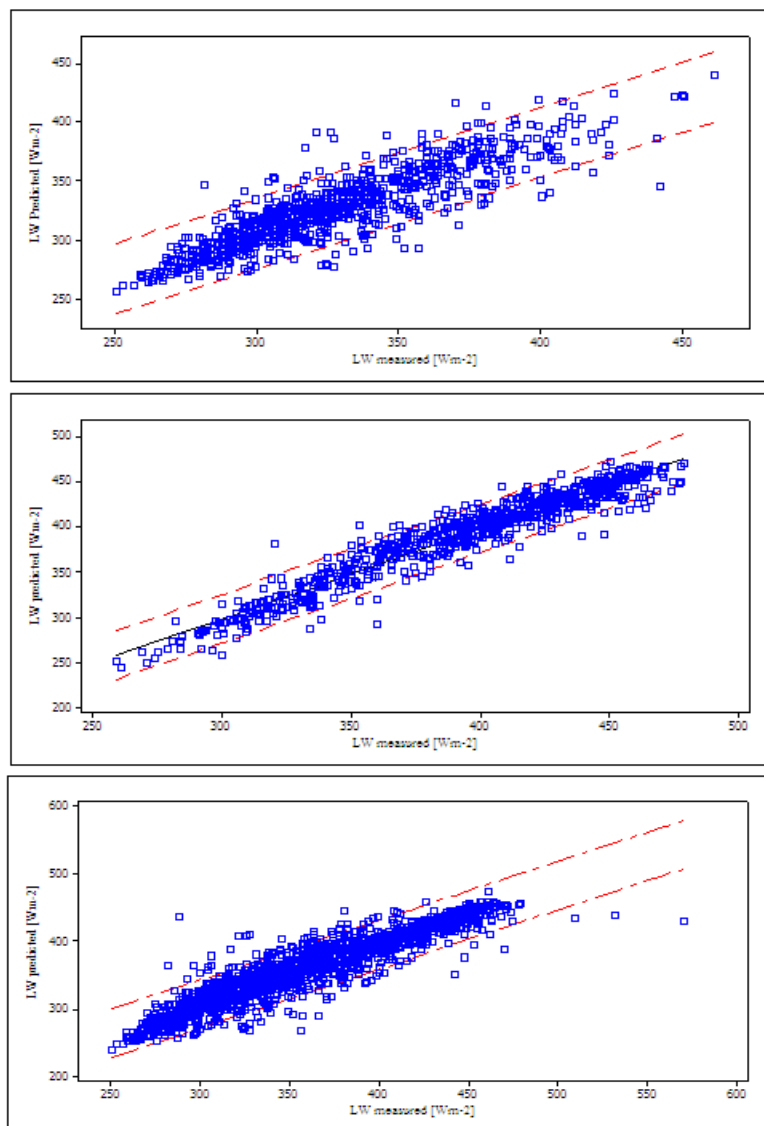


Figure 9. Scatter plot of the measured LW radiation and values predicted using Equation (5-7). The dashed red lines represent the 95% confidence interval.

3.5 Comparisons with Some Existing Parameterizations

Several empirical models from geographical locations around the world have been developed to estimate the LW based on easy-to-measure meteorological variables. These schemes differ from each other in terms of the variables they use, their functional form, and the atmospheric conditions where they were developed.

In this section, 19 clear sky models will be used to evaluate predictions of LW radiation data in Riyadh, Adelaide, and the combined data from both sites. The selected models were chosen for the differences in the variables being used and their functional forms.

Table 4 presents the selected models, their function forms, and the calculated statistical indicators for the three datasets. It can be seen that the predictions of these models differ from one site to another. While some models give adequate predictions for one site, they fail in others. However, some models present reasonable estimates when the measured data are combined from both sites.

For the Riyadh site, the RMSE, MBE and MPE were between 60.65 Wm⁻² and 21.5 Wm⁻², 56 Wm⁻² and 7.7 Wm⁻², and 13% and 1.7% respectively. Based on their statistical indicators, models 1, 4, 10, 12, and 15 gave satisfactory predictions for the measured LW radiation data in Riyadh. However, models 2, 5, 11, and 17 showed poorer predictions according to their statistical values.

The overall predictions of the selected models for the measured data are better for Adelaide than for Riyadh. The RMSE ranges between 35.93 Wm⁻² and 21.46 Wm⁻², MBE varies between -1.33 Wm⁻² and 28.3 Wm⁻², and MPE remains between 8.66% and -0.63. Models 1, 3, 4, 6, 10, and 15 have better statistical indicators for predicting the measured data in comparison with models 2, 5, 7, 10, 11, and 17.

When predicting the measured LW radiation using data from both sites are combined, the best estimate was achieved by model 1 (MBE = -2.57 Wm⁻², MPE = -1.21%, and RMSE 22.55 Wm⁻²) followed by model 4 (MBE = -3.06 Wm⁻², MPE = -1.33%, and RMSE 22.76 Wm⁻²), model 10 (MBE = 3.89 Wm⁻², MPE = 2.55%, and RMSE 26.83 Wm⁻²), model 12 (MBE = -2.57 Wm⁻², MPE = -1.86%, and RMSE 22.41 Wm⁻²), and model 15 (MBE = 4.54 Wm⁻², MPE = 0.87%, and RMSE 24.07 Wm⁻²).

The rest of the models under- or overestimated the measured values to various extents.

Table 4. Author(s) and functional forms of the selected models. MBE, MPE, RMSE values are given for the three datasets.

No	Name	Equation	Riyadh			Adelaide			Both sites		
			MBE	MPE	RMS E	MBE	MPE	RMS E	MBE	MPE	RMS E
1	Angstrom (1915)	$\epsilon_{sky} = 0.82 - 0.25 \times 10^{(-0.168 \times e)}$	7.74	1.78	21.98	7.76	2.72	22.83	2.57	1.21	22.55
2	Brunt (1932)	$\epsilon_{sky} = 0.52 + 0.065 \times \sqrt{e}$	56.98	14.30	60.65	26.75	8.08	34.41	36.88	10.16	44.94
3	FAO (1990)*	$\epsilon_{sky} = 0.64 + 0.044 \times \sqrt{e}$	27.10	6.70	33.37	4.88	1.28	21.46	12.33	3.10	26.06
4	Efmova (1961)	$\epsilon_{sky} = 0.746 + 0.0066 \times e$	9.58	2.24	21.72	9.43	3.13	23.26	3.06	1.33	22.76
5	Garratt (1992)	$\epsilon_{sky} = 0.79 - 0.17 \times e^{-0.96e}$	53.19	13.34	56.80	27.89	8.35	34.66	36.37	10.02	43.36
6	Swinbank (1963)	$\epsilon_{sky} = 9.365 \times 10^{-6} \times T^2$	24.02	5.61	45.55	3.55	0.97	30.43	10.41	2.52	36.20
7	Idso & Jackson (1969)	$\epsilon_{sky} = 1 - 0.261 \times \exp[-0.000777(273 - T)]^2$	44.14	10.99	49.35	24.98	7.32	33.36	31.39	8.55	39.44
8	Ohmura (1981)	$\epsilon_{sky} = 8.733 \times 10^{-3} \times T^{0.788}$	13.08	3.39	28.38	10.66	3.12	25.97	13.54	4.15	25.69
9	Brutsaert (1975)	$\epsilon_{sky} = 1.24 \times \left(\frac{e}{T}\right)^{1/7}$	42.20	10.50	47.35	11.23	3.26	24.85	21.61	13.65	34.09
10	Jin (2006) (Brutsaert)**	$c = 0.0003 \times (T - 273.16)^2 - 0.0079 \times (T - 273.16) + 1.2983$	6.38	2.00	30.03	2.64	0.81	25.06	3.89	2.55	26.83
11	Kruk (2010)	$\epsilon_{sky} = 0.576 \times \left(\frac{e}{T}\right)^{0.202}$	61.05	15.28	66.07	22.34	6.73	33.37	35.31	22.45	46.93

12	Satterlund(1979)	$\epsilon_{sky} = 1.08 \times [1 - \exp(-e^{T/2016})]$	8.35	1.98	21.55	-8.07	-2.72	22.83	-2.57	-1.86	22.41
13	Clark & Allen(1978)	$\epsilon_{sky} = 0.787 + 0.764 \ln\left(\frac{T_{dp} + 273}{273}\right)$	10.62	2.51	22.51	-5.68	-2.03	21.82	23.08	-0.53	23.08
14	Berdhal & Martin (1984)	$\epsilon_{sky} = 0.711 + 0.56 \times \left(\frac{T_{dp}}{100}\right) + 0.73 \times \left(\frac{T_{dp}}{100}\right)^2$	41.42	10.34	46.32	15.40	4.57	26.44	23.92	6.46	35.60
15	Berger 1984	$\epsilon_{sky} = 0.77 + 0.0038 \times T_{dp}$	17.19	4.18	26.01	-1.64	-0.76	20.97	4.54	0.87	24.07
16	Herrero 2012	$\epsilon_{sky} = -1.17 + 0.16 \times RH + 0.0062T$	7.94	2.57	22.18	28.35	8.66	35.93	28.88	8.51	41.05
17	Dilley & O'Brien (1998)	$L_{clr} = 59.38 + 113.7 \times \left(\frac{T}{273.16}\right)^6 + 96.96 \times \sqrt{\frac{PWV}{25}}$	52.27	13.00	56.31	18.84	5.45	28.27	30.04	7.98	39.92
18	Prata(1996)**	$\epsilon_{sky} = 1 - (1 + IWW) \times \exp[-(1.2 + 3 \times IWW)^{0.5}]$	36.88	7.73	36.88	6.33	1.72	21.88	14.68	3.73	27.83
19	Dupont et al. (2008)	$\epsilon_{sky} = \frac{1.2 \times \left(\frac{e}{T}\right)^{1/7}}{0.0492 \times \log\left(\frac{(e/T)^2}{IWW} \times 10^4\right) + 0.88}$	25.43	6.24	32.53	-1.33	-0.63	21.73	7.64	1.67	25.85

*This is a modified version of Brunt's model, as adopted by FAO (REF)

**This model is a modified version of Brutsaert's (1975) model. Jin et al. (2006) have suggested an empirical formula to calculate the constant c, which was taken as 1.24 in the original Brutsaert (1975) model

*** This is the total atmospheric content calculated from $IWW = 0.465 \times \left(\frac{e}{T}\right)$ cm, as proposed by the author of the model

The inaccurate predictions made by some of the selected models highlights that they were developed for sites with atmospheric conditions different from those found in the two considered sites. Likewise, the good performance of some of the models shows that these models were developed under similar atmospheric conditions to those found at the individual sites or both sites.

Furthermore, it is obvious that some of the selected models yield great diversity in their predictions, although they contain the same variable with different forms. For instance, the Swinbank (1963) model (which uses the screen level temperature) and Berdhal and Martin's (1984) formula (which uses the dew point temperature) failed to predict the measured LW radiation accurately for the three datasets, whereas the Satterlund (1979) and Berger (1984) schemes, which have the same variables, gave better predictions.

IV. Conclusions

In this study of longwave radiation, measurements of the temperature, water vapour pressure, and precipitable water vapour at two sites (Adelaide, South Australia, and Riyadh, Central Saudi Arabia) with different atmospheric conditions were used to characterize the monthly and daily variations and to investigate the relationship between LW radiation and these three meteorological variables.

Several conclusions may be drawn from this study:

- 1- LW radiation at both sites follows the trend in temperature, which reaches a maximum in summer and a minimum in winter. The monthly variations in LW radiation, temperature, vapour pressure and PWV, were 36%, 24% and 146% respectively; these values were 78% in Riyadh and 22%, 158%, 59%, and 45% in Adelaide.
- 2- While the amount of LW radiation is confined to a small range (2%–4%) during winter and summer, it varies considerably (8%–12%) during the transition seasons (spring and autumn) at both sites.
- 3- For both sites, the maximum LW radiation values were reached around midday and the minimum values occurred in the early morning. The daily variations in the LW radiation were 13.5% in Riyadh and 10% in Adelaide.

- 4- For both sites, the screen temperature shows better correlation with LW radiation than the screen level water vapour pressure. The latter parameter may not be a suitable measure of the atmospheric water content at all times due to the night/day variations in the height of the atmospheric boundary layer. The relationship between the LW radiation and water content is improved when the precipitable (total, integrated across the whole atmospheric profile) water vapour was used instead.
- 5- Two types of multivariable models have been suggested for predicting the LW radiation, for each site individually and for the combined data from both sites. The first type includes models that use temperature and water vapour pressure at screen level (T, e); the second type uses screen temperature and PWV (T, PWV). Both categories make good predictions of the measured data, although the type which uses (T, PWV) gives better predictions for the three datasets than the model that uses (T, e).
- 6- Nineteen models are selected from previously developed approaches found in the literature, with different functional forms and different meteorological variables; these were used to calculate the measured data for the three datasets (Adelaide, Riyadh, and the combined data from both sites). We find that the predictability of these models varies between dataset and another. Although some models give adequate predictions for one site, they fail for the other. However, some models give reasonable estimates when the measured data from both sites are combined.

Acknowledgements

We would like to thank King Abdulaziz City for Science and Technology (KACST) for supporting this work.

References

- [1]. Alados-Arboledas, L., and J. I. Jimenez, Day-night differences in the effective emissivity from clear skies. *Bound.-Layer Meteor.* 1988, **45**, 93–101.
- [2]. Angstrom A. A study on radiation of the atmosphere, *Smithsonian Misc. Coll.* 1915; 65: 57–69
- [3]. Barbaro, E., A.P. Oliveira, J. Soares, G. Codato, M.J. Ferreira, P. Mlakar, M.Z. Božnar, and J.F. Escobedo, Observational Characterization of the Downward Atmospheric Longwave Radiation at the Surface in the City of São Paulo. *J. Appl. Meteor. Climatol.*, 2010, **49**, 2574–2590,
- [4]. Berdahl P and Fromberg P. The thermal radiance of clear skies, *Sol. Energy.* 1982; 29: 299–314.
- [5]. Berdahl P, Martin M. Emissivity of clear skies. *Sol. Energy.* 1984; 32: 663–664.
- [6]. Berger X, Buriot D, Garnier F. About the equivalent radiative temperature for clear skies, *Solar Energy.* 1984; 32: 725–733.
- [7]. Bilbao J, De Miguel AH. Estimation of daylight downward longwave atmospheric irradiance under clear-sky and all-sky conditions, *J. Appl. Meteorol. Climatol.* 2007; 46: 878–889.
- [8]. Brunt D. Notes on radiation in the atmosphere, *Quart. J. Roy. Meteor. Soc.* 1932; 58: 309–420.
- [9]. Brutsaert W. On derivable formula for long-wave radiation from clear skies. *Water Resour. Res.* 1975; 11: 742–744.
- [10]. CG1 handbook. CG1 pyrgeometer. Instruction manual. Kipp & Zonen. (2000). Delft, Holland.
- [11]. CG4 handbook. CG4 pyrgeometer. Instruction manual. Kipp & Zonen. (2013). Delft, Holland.
- [12]. Clark G, Allen CP. The estimation of atmospheric radiation for clear and cloudy skies. In: *Proc. 2nd Nat. Passive Solar Conf.* 1978; 2: 676–682.
- [13]. Crawford TM, Duchon CE. An improved parameterization for estimating effective atmospheric emissivity for use in calculating daytime downwelling long-wave radiation, *J. Appl. Meteorol.* 1999; 38: 474–480.
- [14]. Culf AD, Gash J. Longwave radiation from clear skies in Niger: a comparison of observations with simple formulas. *J. Appl. Meteorol.* 1993; 32: 539–547.
- [15]. Dilley AC, O'Brien DM. Estimating downward clear sky long-wave irradiance at the surface from screen temperature and precipitable water, *Q. J. R. Meteorol. Soc.* 1998; 124: 1391–1401.
- [16]. Duarte HF, Dias NL, Maggioletto S R. Assessing daytime downward longwave radiation estimates for clear and cloudy skies in southern Brazil. *Agric. For. Meteorol.* 2006; 139: 171–181.
- [17]. Dupont JC, Haeffelin M, Drobinski P, Besnard T. Parametric model to estimate clear-sky longwave irradiance at the surface on the basis of vertical distribution of humidity and temperature, *J. Geophys. Res.* 2008; 113, D07203.
- [18]. Efimova NA. On methods of calculating monthly values of net longwave radiation, *Meteorol. Gidrol.* 1961; 10: 28–33.
- [19]. Emmanuel Sicart, Jean & Hock, Regine & Ribstein, Pierre & Philippe Chazarin, Jean. Sky longwave radiation on tropical Andean glaciers: Parameterization and sensitivity to atmospheric variables. *Journal of Glaciology.* 2010, 56: 854–860.
- [20]. FAO, 1990. Annex V. FAO Penman-Monteith formula. Food and Agriculture Organization of the United Nations, Rome.
- [21]. Heitor, A, Biga AJ, Rosa R. Thermal radiation components of the energy balance at the ground. *Agric. For. Meteorol.* 1991; 54: 29–48.
- [22]. Idso SB, Jackson RD. Thermal radiation from the atmosphere. *J. Geophys. Res.* 1969; 74: 5397–5403.
- [23]. Jin Xin, Barber D, and Tim Papakyriakou, A new clear-sky downward longwave radiative flux parameterization for Arctic areas based on rawinsonde data, *J. Geophys. Res.* 2006, 111, D24104.
- [24]. Kjaersgaard JH, Plauborg FL, Hansen S. Comparison of models for calculating daytime long-wave irradiance using long term data set, *Agric. For. Meteorol.* 2007; 143: 49–63.
- [25]. Kruk, S., Vendrame, F., Rocha, R, Chou, C., Cabral, O. Downward longwave radiation estimates for clear and all-sky conditions in the Sertãozinho region of São Paulo, Brazil. *Theoretical and Applied Climatology.* 2010. 99, v. 115–123.
- [26]. Lhomme JP, Vacher JJ, Rocheteau A. Estimating downward long-wave radiation on the Andean Altiplano. *Agric. For. Meteorol.* 2007; 145: 139–148.
- [27]. Maghrabi, A.H. and Clay, R.W. Precipitable water vapour estimation on the basis of sky temperatures measured by a single-pixel IR detector and screen temperatures under clear skies; 2010; *Journal of meteorological Application*; 2010, 17; 279–286.
- [28]. Maghrabi A. H, 2012, Modification of the IR sky temperature under different atmospheric conditions in an arid region in central Saudi Arabia: Experimental and theoretical justification, *Journal of Geophysical Research.* 2012. 117, D19207.
- [29]. Miskolczi F. Modeling of downward surface longwave flux density for global change applications and comparison with pyrgeometer measurements. *J. Atmos. Ocean. Tech.* 1993, 11, 608–612.

- [30]. Ohmura A. Climate and energy balance of the Arctic tundra. *Züricher Geogr. Schr.* 1981; 3: 448-453.
- [31]. Philipona R, Dutton EG, Stoffel T, Michalsky J, Reda I, Stifter A, Wendling P, Wood N, Clough S.A, Mlawer EJ, Anderson G, Revercomb HE, Shippert TR. Atmospheric longwave irradiance uncertainty: pyrgeometers compared to an absolute sky-scanning radiometer, atmospheric emitted radiance interferometer, and radiative transfer model calculations. *J. Geophys. Res.* 2001; 106 (D22): 28 129– 28 141.
- [32]. Prata A J. A new long-wave formula for estimating downward clear-sky radiation at the surface, *Quart. J. Roy. Meteor.Soc.* 1996; 122: 1127-1151.
- [33]. Riodran D, Clay R , Maghrabi A H, Dawson B, Wild N. Cloud base temperature measurements using a simple longwave infrared cloud detection system, *J. Geophys. Res.* 2006; 110,D03207,doi:10.1029/2004JD005390.
- [34]. Ruckstuhl C, Philipona R, Morland J, Ohmura A. Observed relationship between surface specific humidity, integrated water vapor, and longwave downward radiation at different altitudes, *J. Geophys. Res.*2007; 112, D03302.
- [35]. Satterlund D R. An improved equation for estimating long-wave radiation from the Atmosphere. *Water Resource.Res.*, 1979;15(6): 1649-1650.
- [36]. Skye instrument, 2013: <http://www.skyeinstruments.info/minimet%20main%20menu.htm>.
- [37]. Stephens GL. The parameterization of radiation for numerical weather prediction and climate models. *Monthly Weather Rev.* 1984;112:826–67.
- [38]. Sugita M and Brutsaert W. Cloud Effect in the Estimation of Instantaneous Downward Longwave Radiation, *Water Resource Res.* 1993; 29: 599–605.
- [39]. Swinbank W C. Long-wave radiation from clear skies, *Quart. J. Roy. Meteor. Soc.* 1963; 89:339–48.
- [40]. ViAdez-Mora, A., J. Call* J. A. Gonzalez, and M. A. Jimenez Modeling atmospheric longwave radiation at the surface under cloudless skies, *J. Geophys.Res.*2009, 114, D18107.
- [41]. Wild, M., A. Ohmura, H. Gilgen, J-J. Morcrette, and A. Slingo. Evaluation of Downward Radiation in General Circulation Models, *Journal of Climate.*2001, 14.3227-3229.

Maghrabi A.H. " Monthly and Daily Variations Indownward Longwave Radiation and Its Relationship with Atmospheric Temperature and Water Content Indesert and Mediterranean Climates." *IOSR Journal of Environmental Science, Toxicology and Food Technology (IOSR-JESTFT)* 13.1 (2019): 44-56.